ACS Energy LETTERS

http://pubs.acs.org/journal/aelccp

LETTER

A Neutral pH Aqueous Organic–Organometallic Redox Flow Battery with Extremely High Capacity Retention

Eugene S. Beh,[†,‡] Diana De Porcellinis,[†,#] Rebecca L. Gracia,[∥] Kay T. Xia,[∥] Roy G. Gordon,[*,†,‡] and Michael J. Aziz[*,†]

[†]John A. Paulson School of Engineering and Applied Sciences, Harvard University, Cambridge, Massachusetts 02138, United States
[‡]Department of Chemistry and Chemical Biology, Harvard University, Cambridge, Massachusetts 02138, United States
[#]Department of Chemical Science and Technologies, University of Rome "Tor Vergata", 00133 Rome, Italy
[∥]Harvard College, Cambridge, Massachusetts 02138, United States

Supporting Information

ABSTRACT: We demonstrate an aqueous organic and organometallic redox flow battery utilizing reactants composed of only earth-abundant elements and operating at neutral pH. The positive electrolyte contains bis((3-trimethylammonio)propyl)-ferrocene dichloride, and the negative electrolyte contains bis(3-trimethylammonio)propyl viologen tetrachloride; these are separated by an anion-conducting membrane passing chloride ions. Bis(trimethylammoniopropyl) functionalization leads to ∼2 M solubility for both reactants, suppresses higher-order chemical decomposition pathways, and reduces reactant crossover rates through the membrane. Unprecedented cycling stability was achieved with capacity retention of 99.9943%/cycle and 99.90%/day at a 1.3 M reactant concentration, increasing to 99.9989%/cycle and 99.967%/day at 0.75–1.00 M; these represent the highest capacity retention rates reported to date versus time and versus cycle number. We discuss opportunities for future performance improvement, including chemical modification of a ferrocene center and reducing the membrane resistance without unacceptable increases in reactant crossover. This approach may provide the decadal lifetimes that enable organic–organometallic redox flow batteries to be cost-effective for grid-scale electricity storage, thereby enabling massive penetration of intermittent renewable electricity.

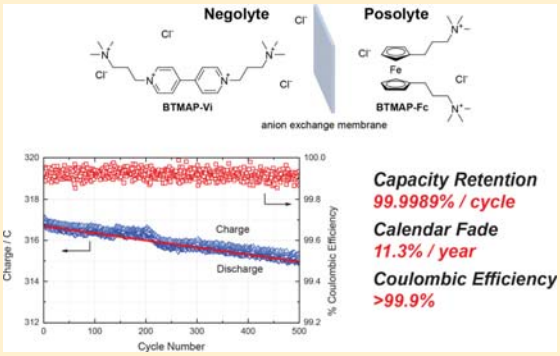

The rapidly falling cost of solar and wind energy generation has paved the way for large-scale adoption; however, storage is of critical importance because of the inherent intermittency of these renewable sources.[1−3] Solid-electrode batteries such as Li-ion are common, but they cannot be discharged cost-effectively for the several hours' duration required for effectively regulating wind and photovoltaic electricity production.[1,2] By storing the electro-active chemical species separately from the power generation stack itself, and pumping the reactants past the electrodes when required, redox flow batteries (RFBs) allow the energy capacity of the entire system to be scaled independently of its maximum power output, thereby offering the promise of cost-effective long-duration discharge.[3,4]

The most popular reactant for RFBs is vanadium, but low earth abundance, high cost, and volatile price limit its widespread commercial adoption.[5] Many other inorganic reactant combinations have been studied, but none have proven more competitive, because of problems such as reactant cost, corrosivity, toxicity, slow kinetics, solubility, energy efficiency, and undesired side reactions.[6,7]

By employing solutions of redox-active organic[8−13] or organometallic[14−19] reactants incorporating only earth-abundant metals, the reactant cost can potentially be lowered substantially while eliminating any concerns about the availability of the reactants when applied to the truly large scales required for grid storage.

In addition to RFBs operating under highly acidic[8] or alkaline[15,16] conditions, several chemistries have been reported that operate at neutral pH, where the low corrosivity is advantageous.[11−13,19] (See Table S1 for a summary of neutral pH aqueous organic RFB chemistries.) However, the reported capacity retentions have still been too low for decadal

Received: January 8, 2017
Accepted: February 7, 2017

DOI: 10.1021/acsenergylett.7b00019
ACS Energy Lett. 2017, 2, 639–644

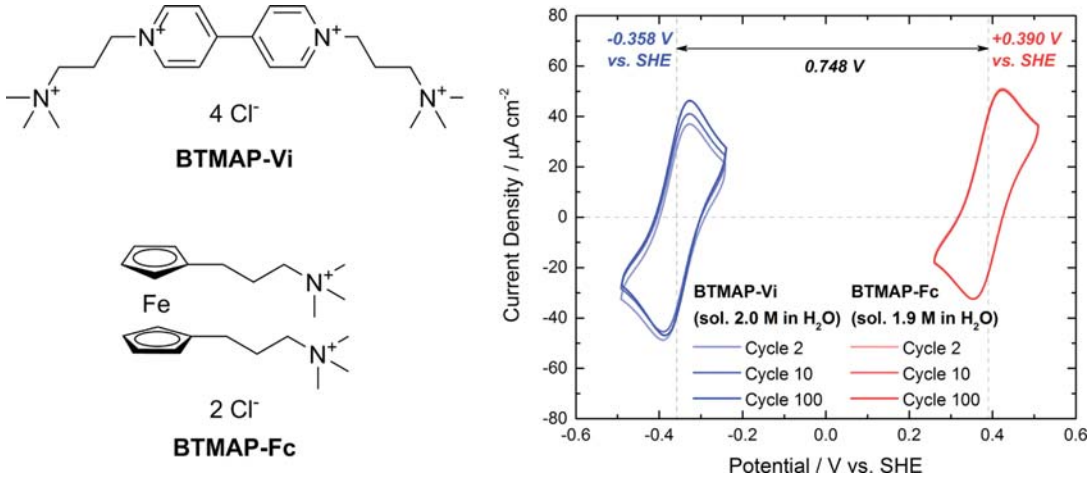

Figure 1. Left: Chemical structures of BTMAP-Vi and BTMAP-Fc. Right: Cyclic voltammograms of BTMAP-Vi (blue trace) and BTMAP-Fc (red trace). The water solubilities and reduction potentials of both molecules vs the standard hydrogen electrode (SHE) are indicated. Note that as BTMAP-Vi is cycled, the solution near the working electrode is gradually depleted of dissolved oxygen. Conditions: 1.0 mM in 0.5 M NaCl, 10 mV s^{-1} sweep rate. The 2nd, 10th, and 100th cycles are superimposed.

operation. Because chemical stability and electrochemical stability are distinct and independent metrics, the capacity retention per cycle reported from rapid cycling experiments does not address calendar-life limitations, which are particularly relevant for molecular reactants. In this Letter, we report a RFB with the highest capacity retention rate to date versus time and versus cycle number. The RFB is operated in water at neutral pH, using organic and organometallic reactants that have very high solubilities (~2 M) in water and do not require any added supporting electrolyte.

The neutral pH organic RFBs reported to date utilize methyl viologen (**MV**) monomers or polymers as the negolyte (negative electrolyte) and typically a nitroxide radical such as (2,2,6,6-tetramethylpiperidin-1-yl)oxyl (TEMPO) in monomeric or polymeric form as the positive electrolyte (posolyte), where chloride ions move across an anion-conducting membrane during operation. A very recent report has introduced water-soluble ferrocene derivatives **FcNCl** and **FcN_2Br_2** (Table S1) in an alternative posolyte for pH 7 RFBs.[19] All three species (viologen, TEMPO, and ferrocene) are susceptible to decomposition via mechanisms that involve the collision of two of the same molecule in a second-order process. (See the Supporting Information for details about the decomposition mechanisms.) This is of particular concern because high reactant concentrations are required in order to achieve high energy densities; indeed, whenever different reactant concentrations have been reported for the same reactant chemistries, lower capacity retention rates have always been observed at higher concentrations of molecular reactants (Table S1).

We therefore designed and synthesized bis(3-trimethylammonio)propyl viologen tetrachloride (**BTMAP-Vi**) as the negolyte and bis((3-trimethylammonio)propyl)ferrocene dichloride as the posolyte (**BTMAP-Fc**; see the Supporting Information). The existence of four positive charges instead of two on the cationic constituent MV^{2+} (for the reduced forms, three vs one for the cation radical $MV^{\bullet+}$) was hypothesized to retard greatly the bimolecular decomposition of **BTMAP-Vi** by a massive increase in the Coulombic repulsion between two molecules compared to $MV^{2+}/MV^{\bullet+}$. A similar effect was hypothesized also to increase the chemical stability of **BTMAP-Fc** compared to **FcNCl**. Both **BTMAP-Vi** and **BTMAP-Fc** are composed of only earth-abundant elements.

In addition to the improved stability of both compounds compared to **MV**, TEMPO, and **FcNCl**, the two positively charged quaternary ammonium groups impart extremely high water solubility to the molecules. For instance, ferrocene is completely insoluble in water, but **BTMAP-Fc** has a solubility of 1.9 M in water at 20 °C; **BTMAP-Vi** has a similar solubility of 2.0 M in water. Moreover, the highly positively charged reactants are expected to also benefit from reduced permeability across anion exchange membranes through enhanced charge and size exclusion.[20] The permeabilities of **BTMAP-Vi** and **BTMAP-Fc** across a Selemion DSV anion exchange membrane were measured to be 6.7×10^{-10} cm^2 s^{-1} and 6.2×10^{-10} cm^2 s^{-1}, respectively (see the Supporting Information). These permeabilities are 5 times lower than **MV**, which was measured at 3.4×10^{-9} cm^2 s^{-1}. From these values, it would take 10.8 and 11.6 years, respectively, for the crossover of **BTMAP-Vi** and **BTMAP-Fc** to lead to a 50% loss in cell capacity.

Rotating disk electrode (RDE) voltammetry measurements (see the Supporting Information) on both reactants gave a reduction rate constant of 2.2×10^{-2} cm s^{-1} for **BTMAP-Vi** and an oxidation rate constant of 1.4×10^{-2} cm s^{-1} for **BTMAP-Fc**, which are much faster than those of common inorganic species,[5] and are also faster than those of most other organic or organometallic reactants[8,9,11,15,16] that have been used in RFBs. The diffusion coefficients for the two reactants were 3.3×10^{-6} and 3.1×10^{-6} cm^2 s^{-1}, respectively.

Figure 1 shows cyclic voltammograms for **BTMAP-Vi** and **BTMAP-Fc** (see the Supporting Information). When used in the negolyte and posolyte in a RFB, respectively, the expected cell potential is 0.748 V. With the high solubilities of both electrolytes in water, the theoretical volumetric capacity (including both electrolytes in the denominator) is 26 Ah L^{-1}, and the theoretical energy density is 20 Wh L^{-1}.

A cell (see the Supporting Information for details) was assembled using 1.3 M **BTMAP-Vi** in water (6.00 mL) as the negolyte and 1.3 M **BTMAP-Fc** in water (6.00 mL) as the posolyte, separated by an anion-conducting membrane (Selemion DSV, 110 μm × 5 cm^2). To prevent atmospheric

DOI: 10.1021/acsenergylett.7b00019
ACS Energy Lett. 2017, 2, 639−644

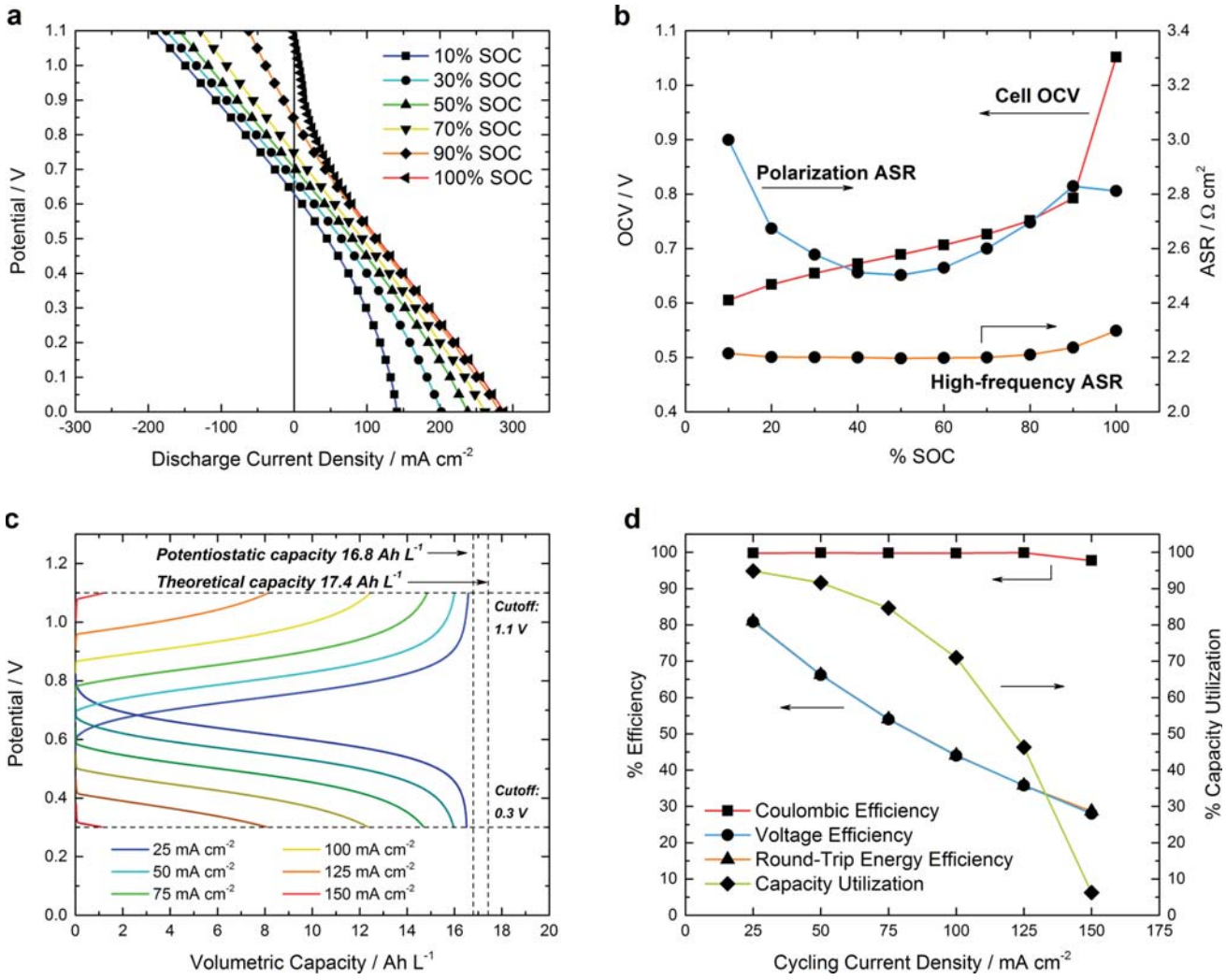

Figure 2. (a) Cell voltage vs discharge current density at 20 °C, at 10%, 30%, 50%, 70%, 90%, and ∼100% SOC. Electrolytes comprise 6.00 mL of 1.3 M BTMAP-Vi (negolyte) and 6.00 mL of 1.3 M BTMAP-Fc (posolyte). (b) Measured cell OCV, high-frequency ASR, and polarization ASR vs SOC. (c) Representative galvanostatic charge and discharge curves from 25 mA cm^{-2} to 150 mA cm^{-2}, in increments of 25 mA cm^{-2}. The vertical dashed lines indicate the maximum volumetric capacity realized with potentiostatic charging and discharging at the indicated voltage cutoffs ("potentiostatic capacity"), as well as the theoretical volumetric capacity. (d) Coulombic efficiency, voltage efficiency, and round-trip energy efficiency (red, blue, and orange traces, left axis), as well as capacity utilization (green trace, right axis) as a percentage of theoretical capacity for cell operation at different current densities.

oxygen from reacting with either electrolyte and promoting decomposition by raising the solution pH, the entire cell was operated inside an argon-filled glovebox. Both electrolyte solutions were also stirred overnight under an argon atmosphere immediately prior to use.

The resulting neutral pH aqueous RFB showed an open-circuit voltage (OCV) that increased nearly linearly from 0.61 V at 10% state of charge (SOC) to 0.79 V at 90% SOC (Figure 2). Polarization studies conducted at room temperature (20 °C) showed a peak galvanic power density of 60 mW cm^{-2} at a current density of 150 mA cm^{-2}. The relatively low peak power and current densities were due in large part to the resistivity of the membrane [∼2.2 Ω cm^2, determined by high-frequency electrochemical impedance spectroscopy (EIS) in the full cell; see the Supporting Information], which was responsible for approximately 75−90% of the area-specific resistance (ASR) of the entire cell (∼2.5 Ω cm^2, DC polarization). Because of the high Coulombic efficiency (99.8−99.9% for current densities of 25−125 mA cm^{-2}), the voltage efficiency dominated the overall round-trip energy efficiency.

An extended charge−discharge study was performed to investigate the stabilities of **BTMAP-Vi** and **BTMAP-Fc** (Figure 3). To minimize the effect of oxygen on capacity retention (see the Supporting Information), the cell was charged to ∼100% SOC and 1.00 mL of posolyte was withdrawn through a syringe. (See the Supporting Information for the cycling performance of a cell operating at a 1:1 reactant molar ratio in oxygen-containing and oxygen-depleted environments and for a comparison with **MV** as the negolyte instead of **BTMAP-Vi**.) The cell was then cycled at a constant current of 50 mA cm^{-2}, with a potential cutoff of 1.1 V while charging and 0.3 V while discharging. The average Coulombic efficiency during galvanostatic cycling was >99.95% (Figure S8). Every 10th cycle, the potential was maintained at the cutoff voltage after galvanostatic charging and discharging until the current dropped below 1 mA cm^{-2}. This allowed the entire capacity of

DOI: 10.1021/acsenergylett.7b00019
ACS Energy Lett. 2017, 2, 639−644

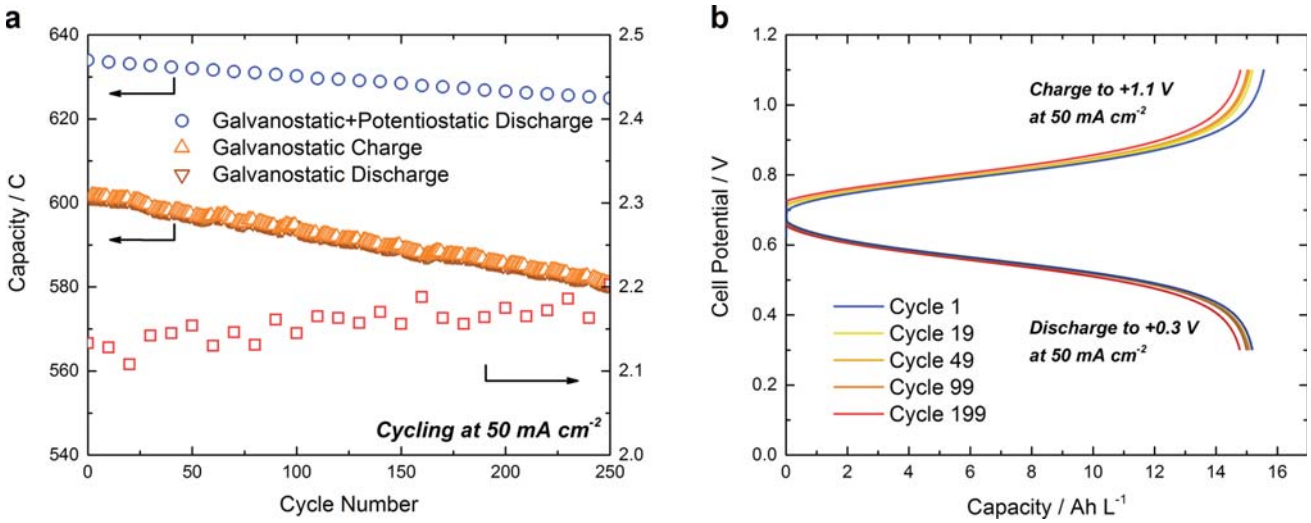

Figure 3. (a) Evolution of the capacity of the BTMAP-Vi/BTMAP-Fc RFB at a concentration of 1.3 M/1.3 M during extended cell cycling at 50 mA cm^{-2} (orange and brown triangles, left axis). At every 10th cycle, the potential was maintained at the end of each charge or discharge until the current fell below 1 mA cm^{-2} (blue circles, left axis). The high-frequency ASR, which was measured immediately after every 10th cycle, is also indicated (red squares, right axis). (b) Representative voltage vs time traces of selected cycles. Cycles that were multiples of (10*n* − 1) were chosen because every 10th cycle was different (see above).

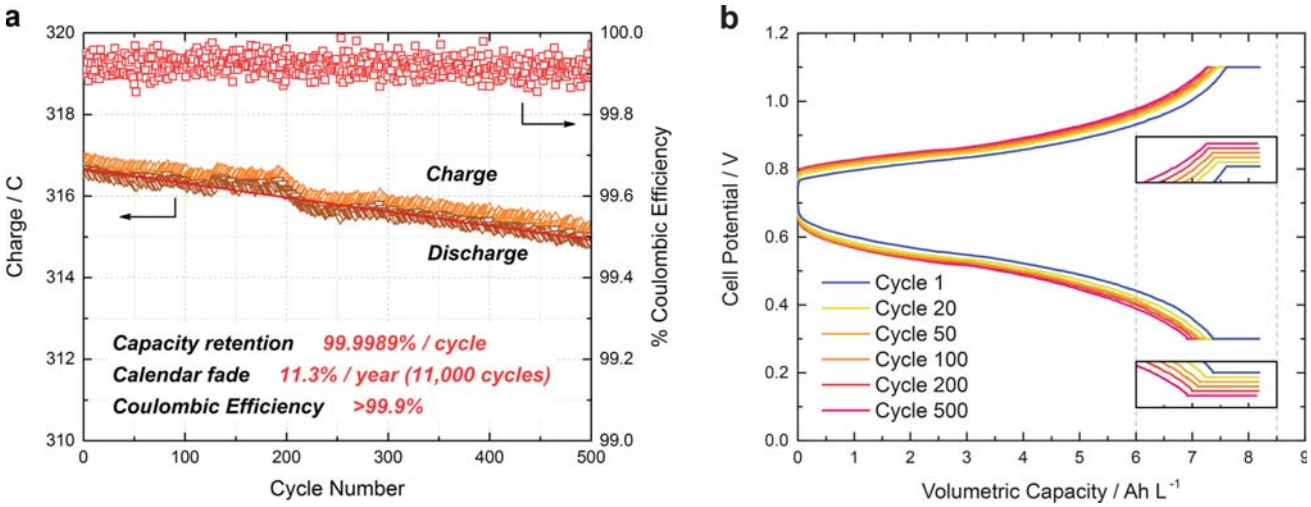

Figure 4. (a) Cycling of a BTMAP-Vi/BTMAP-Fc pH 7 cell at 50 mA cm^{-2} in the presence of an excess of reduced BTMAP-Vi such that the posolyte is capacity-limiting. Bottom traces, left axis: Evolution of the cell charge (upward-pointing triangles) and discharge (downward-pointing triangles) capacity as functions of cycle number. Top trace, right axis: Coulombic efficiency of the cell for each charge−discharge cycle (red squares). The red line is the best fit line to the discharge capacity of the cell between cycles 1 and 500. (b) Representative voltage vs time traces of selected cycles. Inset: Magnification of the potentiostatic regions of each charge−discharge cycle, showing the evolution of the potentiostatic capacity of the cell with cycle number. Inset traces are vertically offset from each other for clarity.

the cell to be measured, independent of any changes to the membrane ASR.

The membrane ASR was measured using potentiostatic EIS at 0.3 V immediately following the potentiostatic discharge from each 10th cycle (i.e., always at ∼0% SOC). The membrane ASR was found to increase very slowly over the course of 2 weeks while showing diurnal variations of ∼0.05 Ω cm^2 depending on the ambient temperature. Changes to the membrane ASR manifested as ripples in the cell capacity with a period of 1 day. Because the ASR slowly increased with time, diminished capacity utilization resulted in a larger apparent decrease in cell capacity over time compared to cycling with a potential hold. Thus, cycling with a potential hold provides a more accurate measure of reactant stability in an operating cell than conventional galvanostatic cycling. In addition, because the potential holds ensure that the entire SOC range is accessed, the cell does not have to achieve a steady-state SOC range, which could otherwise obscure the actual capacity retention rate.

At a concentration of 1.3 M for **BTMAP-Vi** and **BTMAP-Fc**, the cell capacity had fallen to 98.58% of its original value (633.981 to 624.952 C) over 250 cycles (which spanned 14.0 days), representing a capacity retention of 99.9943%/cycle or 99.90%/day. The corresponding capacity fade rates are 0.0057%/cycle and 0.10%/day, respectively. The former figure attributes all of the capacity fade to electrochemical cycling

DOI: 10.1021/acsenergylett.7b00019
ACS Energy Lett. 2017, 2, 639−644

whereas the latter figure attributes it all to chemical decay; thus, these figures represent upper limits if both mechanisms contribute significantly to capacity fade.

Even better capacity retention rates are achievable at lower, but still reasonable, reactant concentrations. Because operation in air led to a very fast drop in cell capacity (see the Supporting Information), another cell was set up inside a nitrogen-filled glovebag with 7.50 mL of 0.75 M **BTMAP-Vi** as the negolyte and 3.25 mL of 1.00 M **BTMAP-Fc** as the posolyte, both at 100% SOC (see the Supporting Information). The glovebag environment contains more oxygen than does the glovebox, but this is mitigated by the excess of reduced **BTMAP-Vi** that is present. This ratio of reactant concentrations was empirically chosen because it minimized water crossover from one reservoir to the other. Next, the cell was cycled for 500 cycles at 50 mA cm^{-2}, this time with a voltage hold after every cycle (Figure 4). The 500 cycles required 16.6 days to complete. The average capacity retention over the 500 cycles was 99.9989%/cycle at an average Coulombic efficiency greater than 99.9%, which reflects a capacity fade rate roughly 3−5 times lower (0.0011%/cycle; 0.033%/day) at the same current density than for the cell described in Figure 3. The corresponding calendar fade rate is 11.3%/year, of which ∼6%/year comes from reactant crossover as calculated from the reactant permeabilities (see above). Compared to the **MV/FcNCl** system, the capacity fade per cycle is reduced by a factor of 10 (vs 0.013%/cycle at 0.5 M) to 40 (vs 0.042%/cycle at 0.7 M) and the capacity fade per day by a factor of 20 (vs 0.58%/day at 0.5 M) to 40 (vs 1.3%/day at 0.7 M), despite still being at a higher reactant concentration.

The calendar fade rate of a **BTMAP-Vi/BTMAP-Fc** cell was found to be independent of the cycling current density (Figure S6), implying that the predominant source of capacity fade is unlikely to be electrochemical decomposition, but rather chemical decomposition or reactant crossover. NMR analyses were performed to evaluate the extent to which chemical decomposition of the reactants at either charge state contributed to capacity loss (see the Supporting Information for details). No trace of either reactant was detectable by NMR in the other reactant reservoir after 250 cycles (at high concentration) or 500 cycles (at lower concentration). Both reactants, in both their oxidized and reduced states, cycled or uncycled, were found by NMR to be stable in aqueous solution. Observed only with experiments in the glovebag but not the glovebox, the dealkylation of **BTMAP-Vi** with hydroxide formed from the reaction of its reduced form with oxygen was identified as a decomposition pathway.

Our experiments imply that as long as oxygen is strictly excluded from the reactants, both **BTMAP-Vi** and **BTMAP-Fc** are electrochemically and chemically stable. From the examples in the literature, the percentage capacity fade rate is generally higher at higher concentrations of reactants, which suggests that a significant portion of the capacity fade is due to bimolecular reactions of the reactants with themselves. Presumably, these pathways are suppressed by the positive charges of BTMAP, which greatly increase the Coulombic repulsion between reactant molecules.

For practical applications, we expect that further improved temporal capacity retention over the already excellent result in Figure 4 will be possible by utilizing a cell design that is better sealed to atmospheric oxygen, or by simply scaling up the volume of the cell. A buffer solution may also be utilized to mitigate any rises in solution pH, though the presence of large anions with low diffusivity from the buffer may potentially raise the cell ASR. Elsewhere, lowering the cell ASR by using more conductive membranes will help to compensate for the relatively low cell voltage, but this should not come at the expense of unacceptably high reactant crossover. Reactant permeabilities were measured in the absence of any external electrical polarization; therefore, reactant crossover in a full cell could be of greater importance than our results suggest.

A complementary strategy is to replace **BTMAP-Vi** with a different molecule that has a lower reduction potential, or using a molecule with a higher reduction potential in place of **BTMAP-Fc**. This will have the effect of raising the cell voltage, peak power density, and energy efficiency of the cell. For instance, diquaternized derivatives of 2,2′-dipyridyl are known to have reduction potentials that are significantly lower (by ∼300 mV) than those of 4,4′-dipyridyl.[21] For an alternative posolyte, we synthesized *N*-((3-trimethylammonio)propyl) ferrocenecarboxamide chloride (**FcCONH-TMAP**; see the Supporting Information) and determined its reduction potential to be +0.63 V vs SHE (+1.04 V vs RHE) at pH 7. This figure is ∼240 mV higher than that of **BTMAP-Fc**, giving a theoretical cell potential of 0.99 V against **BTMAP-Vi**. Because an amide linkage is hydrolyzed in pH 7 water at a rate with a corresponding half-life of several centuries,[22] **FcCONH-TMAP** may be a suitably stable and synthetically accessible replacement for **BTMAP-Fc** in the future.

We have demonstrated an aqueous organic RFB utilizing reactants composed of only earth-abundant elements and operating at pH 7. Functionalization of ferrocene and 4,4′-dipyridyl with BTMAP greatly improves solubility, leading to high realized and theoretical volumetric energy densities of 13 Wh L^{-1} and 20 Wh L^{-1}, respectively, at a cell voltage of 0.748 V. Furthermore, BTMAP functionalization also suppresses reactant crossover through the membrane while ensuring high chemical and electrochemical stability.

The net result is a RFB that cycles stably with unprecedented capacity retention rates. Whether expressed in terms of cycle number or time (99.9989%/cycle; calendar fade rate of 11.3%/year), this capacity retention rate is considerably higher than that for any other RFB chemistry that has been published to date, whether aqueous or nonaqueous, inorganic or organic−organometallic, polymeric or nonpolymeric.

Our extrapolation of the performance of a battery with these properties indicates that if, once every day, it were charged completely over a 5 h period followed by a 5 h complete discharge, we would expect it to retain 50% of its energy storage capacity after 5000 cycles, or about 14 years. The projected capacity retention is anticipated to be an underestimate because as the concentration of active material drops with time, the calendar fade rate will also decrease, i.e., the capacity fade rate has some greater than first-order component. Functionalization of reactants with bulky charged groups represents a promising strategy for developing next-generation aqueous organic RFBs with high capacity and high cycle life.

■ ASSOCIATED CONTENT

Supporting Information

The Supporting Information is available free of charge on the ACS Publications website at DOI: 10.1021/acsenergylett.7b00019.

Table of recent neutral pH aqueous RFB chemistries, additional cell cycling data, decomposition mechanisms

DOI: 10.1021/acsenergylett.7b00019
ACS Energy Lett. 2017, 2, 639−644

of pH 7 RFB reactants, and materials and methods (PDF)

AUTHOR INFORMATION

Corresponding Authors

*E-mail: gordon@chemistry.harvard.edu.
*E-mail: maziz@harvard.edu.

ORCID

Eugene S. Beh: 0000-0002-5746-2973
Michael J. Aziz: 0000-0001-9657-9456

Notes

The authors declare no competing financial interest.

ACKNOWLEDGMENTS

This research was supported initially by ARPA-E Award DE-AR0000348 and subsequently by DE-AC05-76RL01830 through PNNL subcontract 304500. The work was also supported by the Harvard School of Engineering and Applied Sciences and the Massachusetts Clean Energy Technology Center. We thank Prof. Marcel Schlaf, Marc-Antoni Goulet, David Kwabi, Zhengjin Yang, Michael Gerhardt, and Andrew Wong for useful discussions.

REFERENCES

(1) Dunn, B.; Kamath, H.; Tarascon, J. M. Electrical Energy Storage for the Grid: A Battery of Choices. *Science* **2011**, *334*, 928−935.

(2) Yang, Z.; Zhang, J.; Kintner-Meyer, M. C.; Lu, X.; Choi, D.; Lemmon, J. P.; Liu, J. Electrochemical Energy Storage for Green Grid. *Chem. Rev.* **2011**, *111*, 3577−3613.

(3) Nguyen, T.; Savinell, R. F. Flow Batteries. *Electrochem. Soc. Interface* **2010**, 54−56.

(4) Skyllas-Kazacos, M.; Chakrabarti, M. H.; Hajimolana, S. A.; Mjalli, F. S.; Saleem, M. Progress in Flow Battery Research and Development. *J. Electrochem. Soc.* **2011**, *158*, R55.

(5) Weber, A. Z.; Mench, M. M.; Meyers, J. P.; Ross, P. N.; Gostick, J. T.; Liu, Q. Redox Flow Batteries: A Review. *J. Appl. Electrochem.* **2011**, *41*, 1137−1164.

(6) Soloveichik, G. L. Flow Batteries: Current Status and Trends. *Chem. Rev.* **2015**, *115*, 11533−11558.

(7) Winsberg, J.; Hagemann, T.; Janoschka, T.; Hager, M. D.; Schubert, U. S. Redox-Flow Batteries: From Metals to Organic Redox-Active Materials. *Angew. Chem., Int. Ed.* **2017**, *56*, 686−711.

(8) Huskinson, B.; Marshak, M. P.; Suh, C.; Er, S.; Gerhardt, M. R.; Galvin, C. J.; Chen, X.; Aspuru-Guzik, A.; Gordon, R. G.; Aziz, M. J. A Metal-Free Organic-Inorganic Aqueous Flow Battery. *Nature* **2014**, *505*, 195−198.

(9) Yang, B.; Hoober-Burkhardt, L.; Wang, F.; Surya Prakash, G. K.; Narayanan, S. R. An Inexpensive Aqueous Flow Battery for Large-Scale Electrical Energy Storage Based on Water-Soluble Organic Redox Couples. *J. Electrochem. Soc.* **2014**, *161*, A1371−A1380.

(10) Yang, B.; Hoober-Burkhardt, L.; Krishnamoorthy, S.; Murali, A.; Prakash, G. K. S.; Narayanan, S. R. High-Performance Aqueous Organic Flow Battery with Quinone-Based Redox Couples at Both Electrodes. *J. Electrochem. Soc.* **2016**, *163*, A1442−A1449.

(11) Liu, T.; Wei, X.; Nie, Z.; Sprenkle, V.; Wang, W. A Total Organic Aqueous Redox Flow Battery Employing a Low Cost and Sustainable Methyl Viologen Anolyte and 4-HO-TEMPO Catholyte. *Adv. Energy Mater.* **2016**, *6*, 1501449.

(12) Janoschka, T.; Martin, N.; Martin, U.; Friebe, C.; Morgenstern, S.; Hiller, H.; Hager, M. D.; Schubert, U. S. An Aqueous, Polymer-Based Redox-Flow Battery Using Non-Corrosive, Safe, and Low-Cost Materials. *Nature* **2015**, *527*, 78−81.

(13) Janoschka, T.; Martin, N.; Hager, M. D.; Schubert, U. S. An Aqueous Redox-Flow Battery with High Capacity and Power: The TEMPTMA/MV System. *Angew. Chem., Int. Ed.* **2016**, *55*, 14427−14430.

(14) Adams, G. B.; Hollandsworth, R. P.; Webber, B. D. *Rechargeable Alkaline Zinc/Ferricyanide Battery: Final Report for the Period 29 September 1978−28 September 1979*; Lockheed Palo Alto Research Laboratory, Lockheed Missiles & Space Co.: Palo Alto, CA, 1979.

(15) Lin, K.; Chen, Q.; Gerhardt, M. R.; Tong, L.; Kim, S. B.; Eisenach, L.; Valle, A. W.; Hardee, D.; Gordon, R. G.; Aziz, M. J.; et al. Alkaline Quinone Flow Battery. *Science* **2015**, *349*, 1529−1532.

(16) Lin, K.; Gómez-Bombarelli, R.; Beh, E. S.; Tong, L.; Chen, Q.; Valle, A.; Aspuru-Guzik, A.; Aziz, M. J.; Gordon, R. G. A Redox-Flow Battery with an Alloxazine-Based Organic Electrolyte. *Nat. Energy* **2016**, *1*, 16102.

(17) Goeltz, J.; Amadeo, D.; Esswein, A. J.; Jarvi, T. D.; King, E. R.; Reece, S. Y.; Tyagi, N. *Aqueous Redox Flow Batteries Comprising Metal Ligand Coordination Compounds*. U.S. Pat. Appl. 13/948,497, 2014.

(18) Esswein, A. J.; Goeltz, J.; Reece, S. Y.; Madden, T. D.; Amadeo, D.; Jarvi, T. D.; King, E. R. *Aqueous Redox Flow Batteries Featuring Improved Cell Design Characteristics*. U.S. Pat. Appl. 13/796,004, 2014.

(19) Hu, B.; DeBruler, C.; Rhodes, Z.; Liu, T. L. Long-Cycling Aqueous Organic Redox Flow Battery (AORFB) toward Sustainable and Safe Energy Storage. *J. Am. Chem. Soc.* **2017**, *139*, 1207−1214.

(20) Prifti, H.; Parasuraman, A.; Winardi, S.; Lim, T. M.; Skyllas-Kazacos, M. Membranes for Redox Flow Battery Applications. *Membranes (Basel, Switz.)* **2012**, *2*, 275−306.

(21) Krishnan, C. V.; Creutz, C.; Schwarz, H. A.; Sutin, N. Reduction Potentials for 2,2′-Bipyridine and 1,10-Phenanthroline Couples in Aqueous Solutions. *J. Am. Chem. Soc.* **1983**, *105*, 5617−5623.

(22) Smith, R. M.; Hansen, D. E. The pH-Rate Profile for the Hydrolysis of a Peptide Bond. *J. Am. Chem. Soc.* **1998**, *120*, 8910−8913.

EDITOR'S NOTE

The original version of the manuscript was submitted November 4, 2016.

DOI: 10.1021/acsenergylett.7b00019
ACS Energy Lett. 2017, 2, 639−644